metals

MDPI

Article

Influence of Inclusion Parameter and Depth on the Rotating Bending Fatigue Behavior of Bearing Steel

Lijun Xu [1,2], Zhonghua Zhan [1,2,3,*] and Shulan Zhang [4]

[1] Zhongda National Engineering & Research Center of Continuous Casting Technology Co., Ltd., Beijing 100081, China; ljxuah@sina.com
[2] China Iron and Steel Research Institute Co., Ltd., Beijing 100081, China
[3] State Key Laboratory of Advanced Metallurgy, University of Science and Technology Beijing, Beijing 100083, China
[4] Central Lab, Central Iron and Steel Research Institute Company Limited, Beijing 100081, China; zhangshulan@nercast.com
* Correspondence: lyzhan1005@163.com

Abstract: Inclusions are an important parameter affecting the fatigue life of materials. In this paper, the type, size, and quantity of inclusions in bearing steel were quantitatively analyzed using scanning electron microscopy and automatic scanning electron microscopy with an X-ray energy dispersive spectroscopy function. The effects of the inclusion parameters and positions on the rotating bending fatigue properties were analyzed using the rotating bending fatigue test. The results proved that for samples 1 and 2, the inclusions were mainly sulfides, Ti-containing inclusions, and their composite inclusions. For samples 3 and 4, the inclusions were mainly oxides or sulfide–oxide complexes. The number and maximum size of inclusions in sample 2 were relatively small. This was mainly due to the difference in the content of Al, S, and Ca elements in the different samples. The inclusion distance to the surface and the maximum inclusion size had a larger influence on the rotating bending fatigue life in comparison to the inclusion type. Moreover, nitride–oxides had a more detrimental effect on the rotating bending fatigue life as compared to the sulfide–oxide complex inclusions. A model was established on the basis of the inclusion size, depth, and stress by using the Python software. The simulation demonstrated that using five parameters fit well with the experiment results.

Keywords: fatigue; inclusions parameter; GCr15 bearing steel; position

Citation: Xu, L.; Zhan, Z.; Zhang, S. Influence of Inclusion Parameter and Depth on the Rotating Bending Fatigue Behavior of Bearing Steel. *Metals* **2024**, *14*, 907. https://doi.org/10.3390/met14080907

Academic Editor: Ricardo Branco

Received: 30 June 2024
Revised: 1 August 2024
Accepted: 5 August 2024
Published: 9 August 2024

1. Introduction

Fatigue fracturing is the most common failure mode of engineering structures and components in engineering applications [1]. Many studies have focused on the effects of the loading conditions [1,2], microstructure of the materials [3–7], and surroundings [8–13] on fatigue behavior. According to the different material serving conditions, fatigue failure can be classified as axial fatigue, rolling contact fatigue, and rotating bending fatigue. It has been proven that for axial fatigue, fatigue strength is related to the defects with the largest size [2]. Meanwhile, water pressure, temperature, and hydrogen can all influence material fatigue life. In addition, fatigue life is strongly influenced by the microstructure of the material. Yang reports that short fatigue cracks generally originate in ferrite grains or on their boundaries [3]. In addition, it has been observed that larger Al_2Cu precipitates exhibit a higher tendency to fracture than smaller precipitates [4]. In particular, the effect of inclusions or carbides on fatigue behavior has been widely investigated [14–16]. Zhan et al. [17–19] found that a large size of DS inclusions in 15-5PH stainless steel is one of the main causes of fatigue failure, and through thermodynamic software and classical thermodynamic theory calculations of molecular ion coexistence combined with laboratory Al-O equilibrium experiments and slag steel equilibrium experiments, the formation mechanism of large-sized DS inclusions in 15-5PH stainless steel was clarified, and the formation

conditions of large-sized DS inclusions were obtained. The key process parameters that inhibit the formation of large-sized DS inclusions in steel are determined by optimizing the slag composition and the deoxidation process. However, considering the inclusion type, size, and position simultaneously as well as their effect on fatigue behavior is not enough; they need to be discussed systematically.

Bearings are the most vital steel components in modern machinery and are applied in a wide range of fields, such as vehicles, wind turbines, and aerospace. Warhadpande [20] reported that the service conditions, however, can be damaging for the material; such damage can be accelerated by increasing the contact pressure and temperature. For bearings, rolling contact fatigue behavior has been studied thoroughly [6,15,20,21]. In addition, they are always subject to rotating bending stress conditions. Nowadays, fatigue tests are always conducted to evaluate product fatigue properties [3,22]. The rotating bending fatigue behavior of gear steel has been considerably studied in recent years [4,23,24]; however, the effects of the inclusion parameter and its position on the rotating bending fatigue behavior also need to be deeply studied to evaluate bearing fatigue life.

The ASTM E 606 standard covers the determination of low-cycle fatigue properties using uniaxial load specimens. However, the uniaxial test of low-cycle fatigue performance according to the ASTM E 606 [25] standard is usually carried out on a hydraulic testing machine. Due to the inaccurate clamping of the machine, the two ends of the sample can become non-aligned, and there is also a risk of buckling of the sample during compression. Therefore, this paper adopts a rotating bending test method to determine the low-cycle fatigue performance. Compared with uniaxial tensile/compression tests, this type of test can not only avoid the risk of the specimen buckling under compression when a smaller specimen is used, but the test load is also lower because only the outer layer of the specimen section is loaded with the maximum stress [26].

Fatigue life is always predicted based on the cumulative damage rule, local strains, and number of cycles with the consideration of traffic data, in which the relationship between fatigue life and local strain is derived according to the Basquin and Manson–Coffin laws. Up to now, many models have been established to simulate fatigue life for different materials under different operation conditions [27–29]. Due to the great influence of the inclusion type and size on the fatigue life, a model should be established to simulate the fatigue life. However, the co-effect of the inclusion characterization parameter, inclusion size and type, and inclusion distance to surface on the rotating bending fatigue behavior of bearing steel has not been systematically studied in detail. In this paper, the inclusion parameters and their effect on the rotating bending fatigue behavior of bearing steel are deeply investigated. In addition, the rotating bending fatigue life of bearing steel was simulated on the basis of the inclusion characteristic parameter and its position by using the Python software.

2. Experimental Section

Four different batches of GCr15 bearing steel materials were selected for comparative experiments. The contents of Si, Mn, P, Al, Ca, Nb, V, Ti, and Ni in the samples were analyzed by an inductively coupled plasma emission spectrometer (ICP-OES) (iCAPRQ, Thermo Company, Waltham, MA, USA), and the relative standard deviation was ±5%. The content of Cr in the sample was determined using the alkali fusion acid dissolution method. The contents of [C] and [S] in the steel were determined using a high-frequency infrared carbon sulfur analyzer (EMIA-920V2 type). The chemical compositions of the different batches of GCr15 bearing steel are shown in Table 1, and the residual mass fraction is the mass fraction of the Fe element. In the table, it can be seen that the main element contents in the four samples were basically the same, and the contents of the trace elements S, Al, and Ca were different. Among these, the highest content of the S element in sample 1# is 0.004%, the highest content of the Ca element in sample 3# was 0.0005%, and the highest content of the Al element in sample 2# was 0.02%. A large number of studies have shown that the dissolved oxygen content of Al-deoxidized steel is determined by the Al content in

the steel [30]. Therefore, the dissolved oxygen content of sample 2# was the lowest among the four samples.

Table 1. Chemical composition of the tested materials (wt.%).

	C	Si	Mn	P	S	Al	Ca	Nb	V	Ti	Ni	Cr
1#	0.97	0.25	0.32	0.015	0.004	0.01	0.0003	0.003	0.004	0.002	0.01	1.42
2#	0.99	0.23	0.33	0.015	0.003	0.02	0.0004	0.003	0.003	0.002	0.01	1.44
3#	0.98	0.22	0.32	0.017	0.002	0.01	0.0005	0.001	0.003	0.001	0.01	1.48
4#	0.98	0.23	0.33	0.012	0.002	0.01	0.0001	0.003	0.003	0.002	0.01	1.48

To understand the inclusion parameters in the samples, the surface of the steel samples (10 mm × 10 mm × 10 mm) was polished using 2000-mesh SiC paper. Subsequently, the polished samples were mechanically polished using a 5 μm diamond slurry on an automatic polishing machine to achieve a mirror finish. The metallographic samples were scanned and observed by an MLA250 scanning electron microscope combined with an energy dispersive spectrometer, and the types of inclusions were analyzed. To obtain the relationship between the distribution size and chemical composition of the inclusions, the morphology and chemical composition of the inclusions were analyzed using a scanning electron microscope (SEM) and an automated SEM (EVO18-Incasteel, Zeiss Co., Oberkochen, Germany) equipped with X-ray energy dispersive spectroscopy (EDS). The composition characteristics, morphology characteristics, and the size distribution of non-metallic inclusions on the mirror-polished surfaces of steel samples were analyzed. The maximum diameter of an inclusion is defined as its size. The size was set to be greater than 1 μm because the interaction volume could potentially diffuse into the steel and excite electrons from the surrounding environment of the inclusions with diameters smaller than 1 μm.

Standard rotating bending fatigue cylinder specimens were machined to perform the fatigue test under different stresses, and the size of the specimen pattern is shown in Figure 1. In this paper, the values of D, d, L1, L2, and L3 were 6.25 mm, 3 mm, 52 mm, 22 mm, and 15 mm, respectively. The rotating bending fatigue tests were conducted at ambient temperature in air using a rotating bending machine with a stress cycling frequency of 80 Hz and stress ratio R = −1. At least nine specimens of each kind of material were used to measure the fatigue life under different stress levels. After the fatigue tests, the fracture morphologies of all the failure samples were observed by a FEI Quanta650 field emission scanning electron microscope (SEM) and energy dispersive X-ray spectrometer (EDS) at 20 Kv. Finally, the relationship between the type, size, and position of the non-metallic inclusions in the bearing steel and the rotating bending fatigue life was simulated using the Python software.

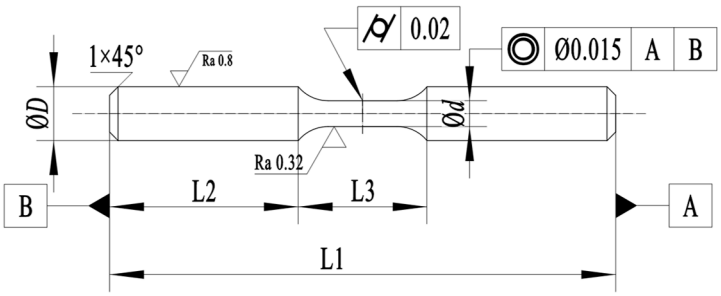

Figure 1. Specimen geometry and size for the rotating bending fatigue test.

3. Results

3.1. Inclusions

The quantity, size, and composition of the inclusions in the four bearing steels were measured separately by the inclusion measurement equipment with an accelerating voltage

of 20 Kv The actual measurement was always different from the setting measurement area because the set area was decided by the two points. Meanwhile, the actual measurement area was ascertained by a certain grid of the same size. Thus, the actual measurement size was always larger than the set area. In this paper, the actual measurement areas of the four samples were 69.12 mm^2, 76.8 mm^2, 69.12 mm^2, and 72.96 mm^2, respectively. The results are shown in Table 2. The results show that the total quantity of inclusions in the measured samples 1#, 2#, 3#, and 4# were 159, 39, 169, and 177, respectively. The inclusion quantity per area and maximum inclusion size in samples 1# and 3# are more and larger. Moreover, it also can be seen that the inclusion in the four bearing steels were mainly Ti carbides or nitrides, sulfides, oxides, and complex sulfides and oxides. However, the main inclusion types were different. For samples 1# and 2#, the inclusions were mainly sulfides and Ti-containing inclusions and its complexes. On the contrary, for samples 3# and 4#, the inclusions were mainly oxides or complexes of sulfides and oxides. Figure 2 shows the inclusion morphology and energy dispersive spectrum (EDS) results of samples 1#, 2#, 3#, and 4#, which were sulfides, oxides, Ti carbides or nitrides, and sulfides and oxides complexes, respectively.

Table 2. The quantity and max size of the different inclusion types in the four bearing steels.

Inclusion Type	Quantity				Max Size (μm)			
	1#	2#	3#	4#	1#	2#	3#	4#
Ti carbides or nitrides	51	9	44	32	9.8	6.1	13.1	11.1
Sulfides	60	18	10	6	18.2	8.7	6.6	6.9
Oxides	3	2	92	34	12.6	14.2	16.7	10.5
Complexes of sulfides and oxides	45	10	23	105	13.3	5.6	12.6	11.3

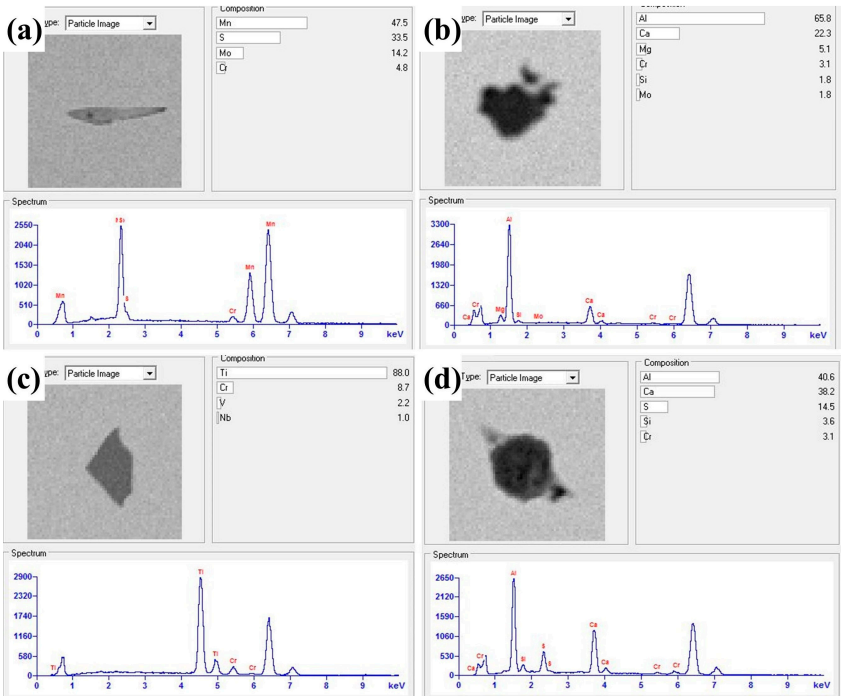

Figure 2. Inclusion images of samples 1#, 2#, 3#, and 4#: (**a**) sulfides in sample 1#; (**b**) oxides in sample 2#; (**c**) Ti carbides or nitrides in sample 3#; (**d**) complexes of sulfides and oxides in sample 4#.

3.2. Fatigue Results

The rotating bending fatigue results of the four samples are shown in Figure 3. The results demonstrate that the number of cycles to failure increased as the cyclic stress decreased. Specifically, the results of number of cycles to failure for the samples under

1400 MPa obviously imply that the maximum number of cycles for sample 2# was larger than the others, and the number of fatigue cycles of sample 1# was the least. Table 2 shows that the quantity and size of the inclusions of sample 2# were the least and smallest, which may be the reason for the larger number of fatigue cycles. However, for samples 1# and 3#, the smaller number of fatigue cycles may be related to the larger inclusion size. In conclusion, the inclusion test results could predict the fatigue properties to some extent. In other words, the rotating bending fatigue behavior can be assessed based on the characteristic parameters of the inclusions.

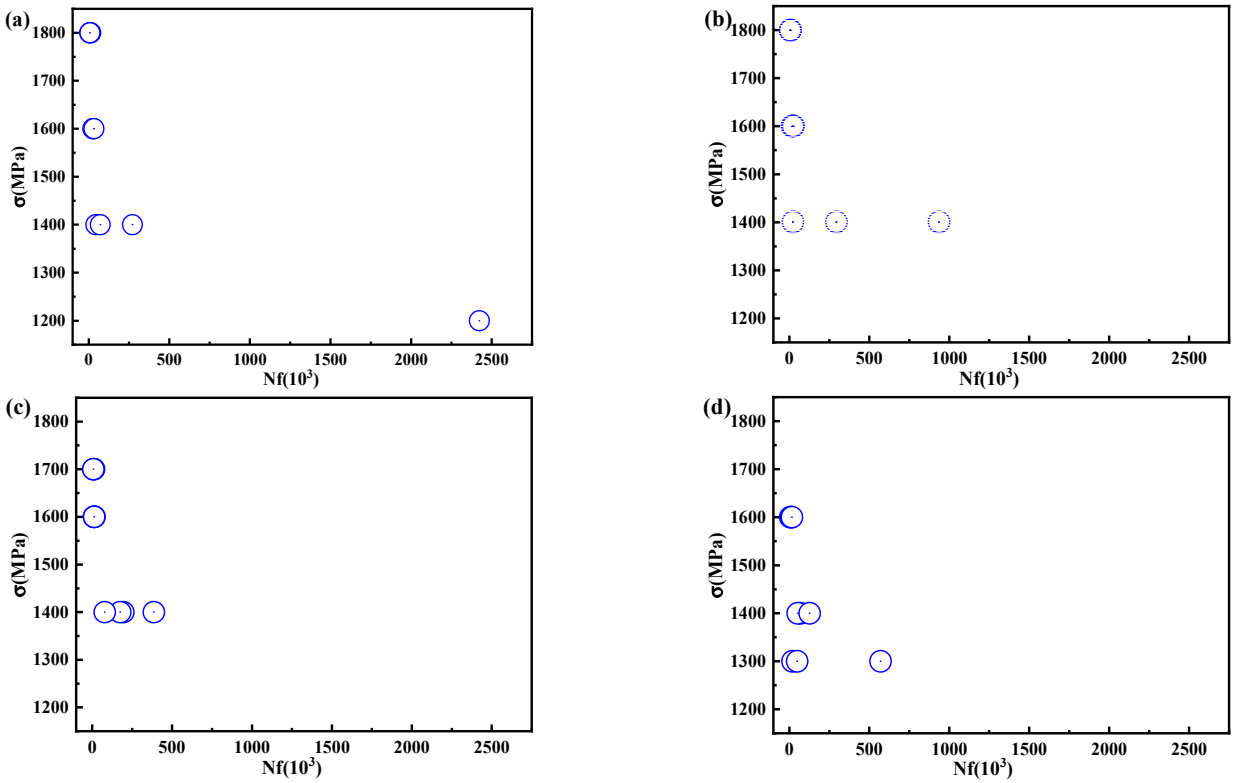

Figure 3. The number of cycles to failure obtained from the rotating bending fatigue tests for samples under different stress: (**a**) sample 1#; (**b**) sample 2#; (**c**) sample 3#; (**d**) sample 4#.

3.3. Fracture Morphology

It has been shown that the distance of inclusions from the surface is another factor influencing the fatigue properties [18]. In order to analyze the fracture initiation source, the fraction morphologies of each rotating bending sample were observed. Furthermore, if an inclusion served as the fracture initiation source, its composition, size, and distance from the surface were measured. Figure 4 displays the fracture morphology of samples 1# and 4# subjected to a stress of 1400 MPa. It can be seen that the inclusions were the crack source and that the inclusion types were different, including Ti-containing inclusions and complex inclusions of oxide and sulfide. The inclusion depths were also measured, which were about 120 μm and 30 μm, respectively, for samples 2# and 4#. Additionally, as can be seen in Figure 4, it is evident that the Ti-containing inclusion size was approximately 10 μm, while the complex inclusion size, comprising oxide and sulfide, was about 15 μm. Combining the analysis of the SEM fracture images and EDS results of the inclusions, all the inclusion types, sizes, and depths were all determined for the samples that involved inclusion-induced fractures during rotating bending test. The high-magnification SEM results (Figure 5) of the fractures for samples 2# and 4# subjected to a cyclic stress of 1400 MPa showed that the fracture morphologies were mostly intergranular fractures and dimple fractures. The morphologies of the two samples were basically the same, indicating that the crack propagation mechanism occurred in the same way once the crack formed. Moreover, apart

from the cracks initiated by the inclusions, for the samples without inclusions or with inclusions far below the surface, the cracks typically initiated from surface defects.

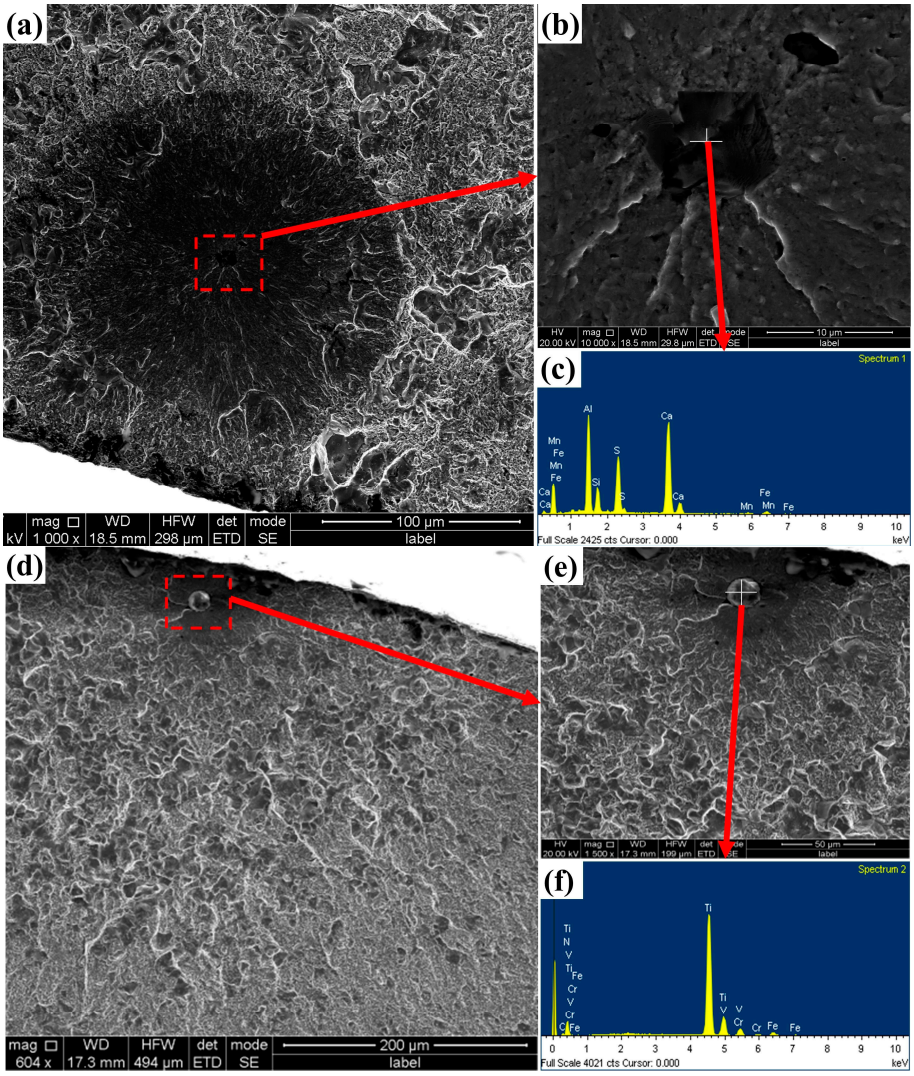

Figure 4. SEM fracture images showing fatigue cracks initiated at inclusions and EDS results of inclusions of samples 2# and 4# subjected to cyclic stress of 1400 MPa: (**a**) sample 2#; (**b**) magnification of Figure (**a**); (**c**) EDS result of (**b**) inclusion of (**e**); (**d**) sample 4#; (**e**) magnification of (**d**); (**f**) EDS result of (**e**) inclusion.

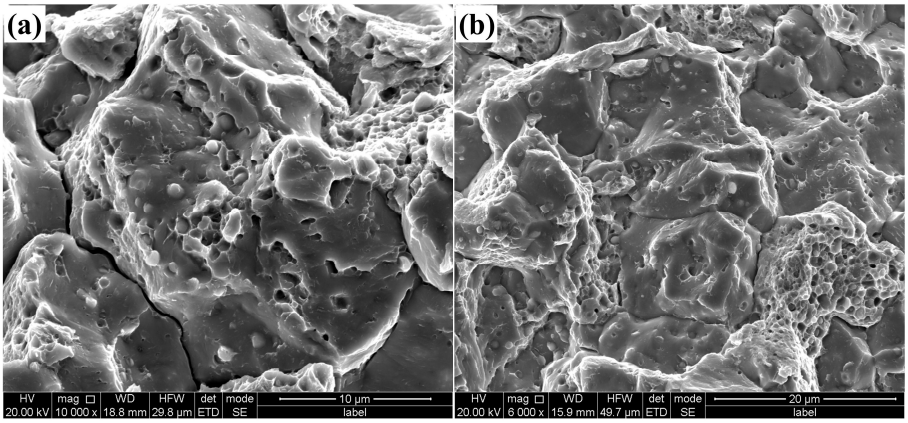

Figure 5. SEM fracture images showing fatigue fracture morphology: (**a**) sample 2#; (**b**) sample 4#.

4. Discussions

It has been reported that cracks can initiate from non-metallic inclusions such as Al_2O_3, and the results of this study were consistent with former results [14]. According to Figures 3–5, it can be concluded that the decrease in the fatigue life was mainly related to the characteristic parameters of the inclusions and surface defects. Regardless of the four kinds of composition differences, the relationship among the fatigue life, inclusion size, and depth are discussed. All the inclusion-initiated rotating bending fatigue cracks are included in Figure 6. This indicates that the number of cycles to failure decreased with the increase in the inclusion size and decrease in depth. In particular, the number of cycles to failure for the samples subjected to a stress of 1300 MPa was smaller than the samples subjected to a stress of 1400 MPa, which was caused by the larger inclusion size and smaller depth. It can be seen from Figure 6a that the depth was about 25 μm, and the maximum inclusion size was larger than 30 μm for the samples subjected to a stress of 1300 MPa. However, for the samples subjected to a stress of 1400 MPa, the maximum inclusion size was about 26 μm, and the minimum depth was smaller than 25 μm; thus, it can be concluded that the inclusion size is a more influential factor in decreasing the fatigue life compared to the depth. This conclusion is consistent with the results shown in Table 2 and Figure 2. The maximum size for sample 1# was the largest, and the fatigue life was the smallest. The equivalent diameter of the largest non-metallic inclusion in Figure 6 of the same sample was larger than the maximum size of the non-metallic inclusion in Table 2. This is because the size of the fatigue sample was much larger than the measured size of the inclusions. However, the measured inclusions results can offer a reference for evaluating the fatigue life.

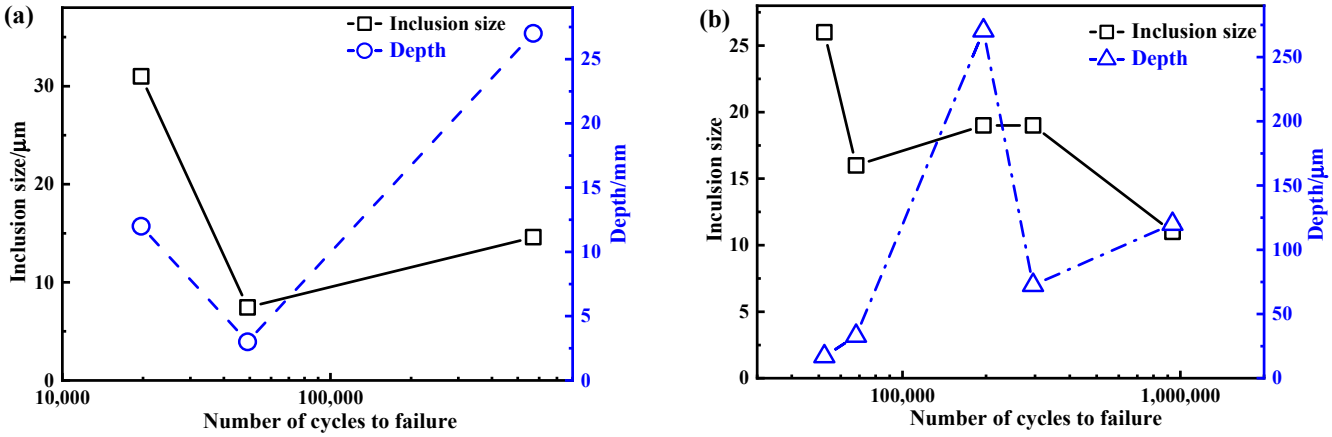

Figure 6. The relationship among number of cycles to failure, inclusion size, and depth for the samples subjected to different stresses: (**a**) 1300 MPa; (**b**) 1400 MPa.

From Table 2, it can be seen that the inclusion type in the four kinds of bearing steels was mainly oxide, Ti-containing inclusions, sulfides, and complexes of sulfide and oxides. The effect of the inclusion type on the fatigue life is also demonstrated in Figure 7. It apparently shows that the maximum inclusion size is a more influential factor in decreasing the fatigue life as compared to the inclusion type. A former investigation proved that Ti-containing nitride is more detrimental to materials in terms of decreasing their fatigue life as compared to sulfides and nitrides. Table 2 shows that the main inclusion types were Ti-containing nitride or carbide, oxides, and complexes of sulfide and oxides. The results shown in Figure 7 also prove that the inclusions that induced fatigue cracks were mainly complexes of sulfide and oxide and Ti-containing inclusions. However, the depth of the Ti-containing inclusions from the surface was smaller, and their size was smaller than 10 μm, which made the fatigue life of the sample comparably larger compared to the sample with inclusions larger than 25 μm. It can be concluded that the maximum inclusion

size is the most detrimental factor in terms of decreasing the rotating bending fatigue life of bearing steels.

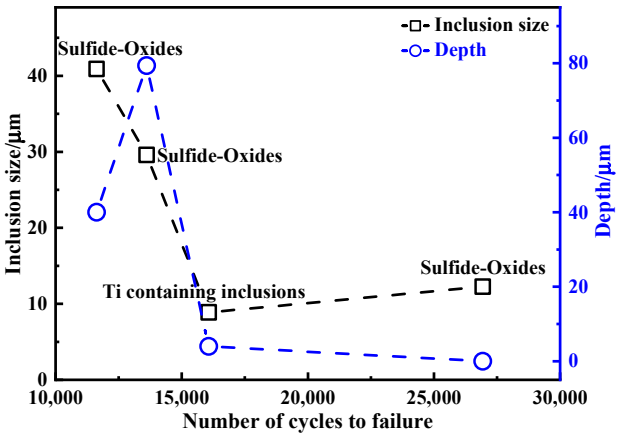

Figure 7. The relationship among number of cycles to failure, inclusion type, and depth for the four kinds of samples subjected to stress of 1600 MPa.

Fatigue life models based on the microstructure and loading conditions have been investigated for many years [21,31–34]. Fu [21] investigated a model based on the white etching areas (WEAs), dark etching regions (DERs), and white etching bands (WEBs) to estimate the bearing rolling contact life using the WEA appearance model. Murakami et al. [34] first proposed the famous area parameter model in combination with the steel hardness and inclusion size to estimate the fatigue strength for a specimen in which fatigue cracks initiated from internal inclusions. The dark area was also named the fine granular area (FGA) by Sakai et al. [35] or the "granular bright facet (GBF)" by Shiozawa et al. [36] when observed by a scanning electron microscope (SEM). Murakami investigated the relationship between the stress intensity factor range ΔK at the crack initiation site and the inclusion size, which can be expressed as follows:

$$\Delta K = C\sigma\sqrt{\pi\sqrt{\text{Area}}} \quad (1)$$

where σ is the applied stress amplitude; C is a constant; and $\sqrt{\text{Area}}$ is the square root of the area of the inclusion or granular bright facet. The equation indicates that the fatigue life decreases with ΔK or the inclusion size. However, in this equation, the inclusion depth is not considered. According to the experiment results in this paper, in addition to the inclusion size and stress amplitude, it can be concluded that the depth is also an important factor that influences the fatigue life. Thus, in this paper, the rotation bending fatigue life based on the inclusion size, depth, and stress was simulated using the Python software for studying the inclusion-induced cracking of bearing steel. The simulation results are shown in Figure 8. The results show that the MSE (mean square error) inclined to zero when the X variable was to the fifth power, which indicates that the simulation results fit well. However, when the X variable was 6–9, the MSE value also inclined to 0, and the computation time was comparably larger. The MSE increased when the highest power increased to 10, which indicates that the simulation results did not correlate well with the power. The MSE is a convex function, and it has a minimum value. In our paper, the value is five. Thus, the fifth power gives the best simulation results. The model is shown in Equation (2).

$$y = \sum_{i=0}^{n} C_i X^n + b \quad (2)$$

where y is the fatigue life; c_i is a constant that can be obtained by the simulation result; and X is the variables. In this paper, the variables are the inclusion size, depth, and stress. MSE represents the variance between the predicted and actual values. The actual value is

the cycle y. The simulation results prove that the five is the best choice. According to the rotating bending fatigue experiment results, c_i and b are shown in Table 3. It is noted that the equation only fits to the inclusion-initiated rotating bending fatigue for bearing steel.

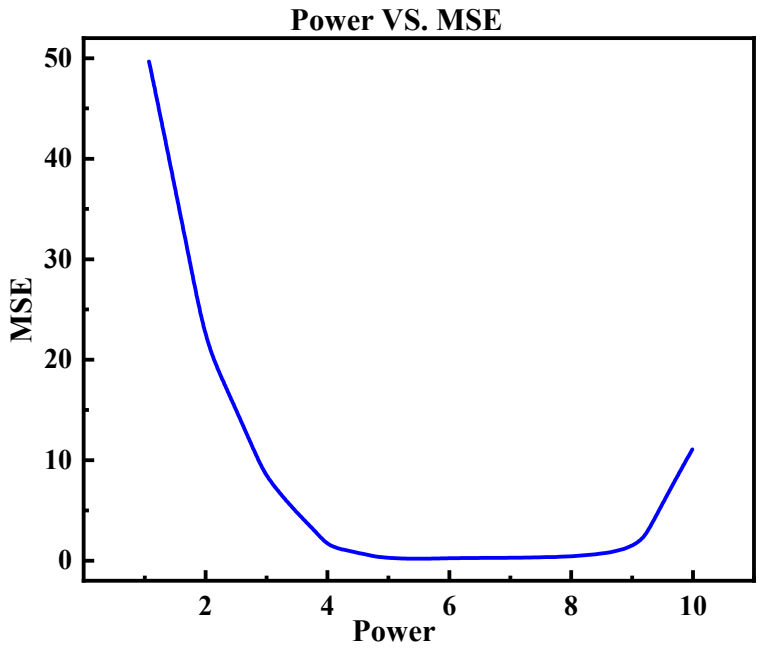

Figure 8. Simulation results for the round and MSE.

Table 3. Simulation results of C_i and b.

	1	2	3
C_1	1715.609	80,533.775	−0.151
C_2	11,685.791	−4456.257	−3.232
C_3	−573.446	77.673	−46.117
C_4	3.697	−0.497	−439.102
C_5	0.089	0.001	23.791
b		3,217,543.924	

5. Conclusions

In this paper, the shape characteristics, distribution characteristics, and composition types of non-metallic inclusions in four different batches of GCr15 bearing steel were analyzed in detail using SEM and energy spectrum analysis. The morphology, composition, and size distribution of the inclusions in the samples were obtained using an automatic inclusion analysis system. Fatigue cycles for the different samples under different load conditions were analyzed using rotating bending fatigue testing machines. Combined with the fracture morphology analysis of all the failed samples, the relationship between the type, size, and position of the non-metallic inclusions in the bearing steel and the fatigue life of rotating bending were simulated using the python software. The following conclusions were drawn:

(1) The inclusion type in the four kinds of bearing steel were mainly Ti carbides or nitrides, sulfides, oxides, and complexes of sulfides and oxides, respectively. For samples 1# and 2#, the inclusions were mainly sulfides and Ti-containing inclusions and its complexes. Conversely, for samples 3# and 4#, the inclusions were mainly oxides or complexes of sulfides and oxides. The inclusion quantity and maximum size of sample 2# were comparably less and smaller. This was mainly attributed to the difference in the content of Al, S, and Ca elements among the samples.

(2) The rotating bending fatigue life for sample 2# was longer, which was consistent with the inclusion measurement results; the inclusion results reflect the material's rotating bending fatigue to some extent. Compared to the inclusion depth and inclusion type, the inclusion size was the most influential factor in reducing the rotating bending fatigue life of the bearing steels.

(3) A simulation was attempted based on the rotating bending fatigue test using the Python software. The results indicated that the rotating bending fatigue cycle could be simulated using polynomials. The variables were the inclusion size, inclusion depth, and stress y. The number of items was five. The coefficient was given.

Author Contributions: Conceptualization, L.X. and Z.Z.; methodology, L.X. and Z.Z.; software, L.X. and Z.Z.; validation, L.X. and Z.Z.; formal analysis, L.X. and S.Z.; investigation, L.X. and Z.Z.; resources, L.X. and Z.Z.; data curation, L.X. and Z.Z.; writing—original draft preparation, L.X. and Z.Z.; writing—review and editing, L.X. and Z.Z.; visualization, L.X. and Z.Z.; supervision, S.Z.; project administration, S.Z.; funding acquisition, L.X. and Z.Z. All authors have read and agreed to the published version of the manuscript.

Funding: This research was funded by the National Natural Science Foundation of China Ministry of Science and Technology, grant number 52204330.

Data Availability Statement: Data are available in a publicly accessible repository.

Conflicts of Interest: Author Lijun Xu and Zhonghua Zhan were employed by the company Zhongda National Engineering & Research Center of Continuous Casting Technology Co., Ltd. and China Iron and Steel Research Institute Co., Ltd. Author Shulan Zhang was employed by the company Central Lab, Central Iron and Steel Research Institute Company Limited. The remaining authors declare that the research was conducted in the absence of any commercial or financial relationships that could be construed as a potential conflict of interest.

References

1. Zhao, L.H.; Feng, J.Z.; Zheng, S.L. Effect of Cyclic Stresses Below the Endurance Limit on the Fatigue Life of 40Cr Steel. *Strength Mater.* **2018**, *50*, 2–10. [CrossRef]
2. Rigon, D.; Meneghetti, G.; Görtler, M.; Cozzi, D.; Waldhauser, W.; Dabalà, M. Influence of Defects on Axial Fatigue Strength of Maraging Steel Specimens Produced by Additive Manufacturing. *MATEC Web Conf.* **2018**, *165*, 02005. [CrossRef]
3. Yang, B.; Dai, S.; Wu, Y.Y.; Liao, Z.; Liang, S.; Xiao, S.N. Short Fatigue Crack Behavior of LZ50 Axle Steel Under Rotating-Bending Cyclic Loading. *Strength Mater.* **2018**, *50*, 193–202. [CrossRef]
4. Kosturek, R.; Śnieżek, L.; Torzewski, J.; Wachowski, M. Low Cycle Fatigue Properties of Sc-Modified AA2519-T62 Extrusion. *Materials* **2020**, *13*, 220. [CrossRef]
5. Ganti, S.; Turner, B.; Kirsch, M.; Anthony, D.; McCoy, B.; Trivedi, H.; Sundar, V. Three-Dimensional (3D) Analysis of White Etching Bands (WEBs) in AISI M50 Bearing Steel Using Automated Serial Sectioning. *Mater. Charact.* **2018**, *138*, 11–18. [CrossRef]
6. Swahn, H.; Becker, P.C.; Vingsbo, O. Martensite Decay during Rolling Contact Fatigue in Ball Bearings. *Met. Metall. Trans. A* **1976**, *7*, 1099–1110. [CrossRef]
7. Voskamp, A.P.; Mittemeijer, E.J. The Effect of the Changing Microstructure on the Fatigue Behaviour during Cyclic Rolling Contact Loading. *Int. J. Mater. Res.* **2021**, *88*, 310–320.
8. An, X.; Shi, Z.; Xu, H.; Wang, C.; Wang, Y.; Cao, W.; Yu, J. Quantitative Examination of the Inclusion and the Rotated Bending Fatigue Behavior of SAE52100. *Metals* **2021**, *11*, 1502. [CrossRef]
9. Karr, U.; Schönbauer, B.M.; Sandaiji, Y.; Mayer, H. Effects of Non-Metallic Inclusions and Mean Stress on Axial and Torsion Very High Cycle Fatigue of SWOSC-V Spring Steel. *Metals* **2022**, *12*, 1113. [CrossRef]
10. Gao, Z.; Pan, G.; Wang, S.; Song, Y.; Wu, H.; Mao, X. Effect of Mg on Inclusion and High Cycle Fatigue Behavior in Titanium Microalloyed Beam Steel. *Metals* **2023**, *13*, 760. [CrossRef]
11. Luo, Y.; Liu, X.; Chen, F.; Zhang, H.; Xiao, X. Numerical Simulation on Crack–Inclusion Interaction for Rib-to-Deck Welded Joints in Orthotropic Steel Deck. *Metals* **2023**, *13*, 1402. [CrossRef]
12. Motte, R.; De Waele, W. An Overview of Estimations for the High-Cycle Fatigue Strength of Conventionally Manufactured Steels Based on Other Mechanical Properties. *Metals* **2024**, *14*, 85. [CrossRef]
13. Nikolic, K.; De Wispelaere, J.; Ravi, G.; Hertelé, S.; Depover, T.; Verbeken, K.; Petrov, R.H. Confirming Debonding of Non-Metallic Inclusions as an Important Factor in Damage Initiation in Bearing Steel. *Metals* **2023**, *13*, 1113. [CrossRef]
14. Grabulov, A.; Ziese, U.; Zandbergen, H.W. TEM/SEM Investigation of Microstructural Changes within the White Etching Area under Rolling Contact Fatigue and 3-D Crack Reconstruction by Focused Ion Beam. *Scr. Mater.* **2007**, *57*, 635–638. [CrossRef]

15. Fu, H.; Galindo-Nava, E.; Rivera-Díaz-del-Castillo, P. Modelling and Characterisation of Stress-Induced Carbide Precipitation in Bearing Steels under Rolling Contact Fatigue. *Acta Mater.* **2017**, *128*, 176–187. [CrossRef]
16. Wang, Z.Y.; Xing, Z.G.; Wang, H.D.; Shan, D.B.; Huang, Y.F.; Xu, Z.H.; Xie, F.K. The Relationship between Inclusions Characteristic Parameters and Bending Fatigue Performance of $20Cr_2Ni_4A$ Gear Steel. *Int. J. Fatigue* **2022**, *155*, 106594. [CrossRef]
17. Zhan, Z.; Zhang, Y.; Shi, R.; Qiao, T.; Wang, G.; Cheng, G. Effect of Slag Basicity on Non-Metallic Inclusions and Cleanliness of 15-5PH Stainless Steel. *Metals* **2023**, *13*, 750. [CrossRef]
18. Zhan, Z.; Zhang, W.; Zhang, Y.; Shi, R.; Cheng, G. Formation and Evolution of DS-Type Inclusions in 15-5PH Stainless Steel. *Metals* **2021**, *11*, 1129. [CrossRef]
19. Zhang, W.; Wang, G.; Zhang, Y.; Cheng, G.; Zhan, Z. Formation Mechanism and Improvement of Magnetic Particle Inspection Defects in Cr5 Backup Roller Forged Ingot. *Metals* **2022**, *12*, 295. [CrossRef]
20. Warhadpande, A.; Sadeghi, F.; Evans, R.D. Microstructural Alterations in Bearing Steels under Rolling Contact Fatigue Part 1-Historical Overview. *Tribol. Trans.* **2013**, *56*, 349–358. [CrossRef]
21. Fu, H.W.; Rivera-Díaz-del-Castillo, P.E. A Unified Theory for Microstructural Alterations in Bearing Steels under Rolling Contact Fatigue. *Acta Mater.* **2018**, *155*, 43–55. [CrossRef]
22. Brnic, J.; Krscanski, S.; Lanc, D.; Brcic, M.; Turkalj, G.; Canadija, M.; Niu, J. Analysis of the Mechanical Behavior, Creep Resistance and Uniaxial Fatigue Strength of Martensitic Steel X46Cr13. *Materials* **2017**, *10*, 388. [CrossRef]
23. Xiao, N.; Hui, W.J.; Zhang, Y.J.; Zhao, X.L.; Chen, Y.; Dong, H. High Cycle Fatigue Behavior of a Low Carbon Alloy Steel: The Influence of Vacuum Carburizing Treatment. *Eng. Fail. Anal.* **2020**, *109*, 104215. [CrossRef]
24. Chen, W.; He, X.F.; Yu, W.C.; Shi, J.; Wang, M.Q.; Yao, K.F. Rotating Bending Fatigue Properties of Case Carburized Steel with Different Fractions of Retained Austenite. *J. Mater. Eng. Perform.* **2023**, *32*, 7960–7968. [CrossRef]
25. *ASTM E606/E606M-12*; Standard Test Method for Strain-Controlled Fatigue Testing. ASTM: West Conshohocken, PA, USA, 2012.
26. Knez, M.; Glodež, S.; Ružička, M.; Kramberger, J. A Rotating Bending Approach for Determination of Low-Cycle Fatigue Parameters. *Int. J. Fatigue* **2010**, *32*, 1724–1730. [CrossRef]
27. Shibanuma, K.; Ueda, K.; Ito, H.; Nemoto, Y.; Kinefuchi, M.; Suzuki, K.; Enoki, M. Model for Predicting Fatigue Life and Limit of Steels Based on Micromechanics of Small Crack Growth. *Mater. Des.* **2018**, *139*, 269–282. [CrossRef]
28. El May, M.; Saintier, N.; Palin-Luc, T.; Devos, O.; Brucelle, O. Modelling of Corrosion Fatigue Crack Initiation on Martensitic Stainless Steel in High Cycle Fatigue Regime. *Corros. Sci.* **2018**, *133*, 397–405. [CrossRef]
29. Liu, Q.; Cai, L.X.; Chen, H.; Bao, C.; Yin, T. A Novel Test Method Based on Small Specimens for Obtaining Low-Cycle-Fatigue Properties of Materials. *Mech. Mater.* **2019**, *138*, 103153. [CrossRef]
30. Zhan, Z.; Wang, G.; Shi, R.; Zhang, W.; Zhang, Y.; Cheng, G. Inclusion Control of 15-5 PH High-Strength Stainless Steel through Aluminum Deoxidation. *ISIJ Int.* **2023**, *63*, 622–630. [CrossRef]
31. Branco, R.; Berto, F.; Zhang, F.C.; Long, X.Y.; Costa, J. Comparative Study of the Uniaxial Cyclic Behaviour of Carbide-Bearing and Carbide-Free Bainitic Steels. *Metals* **2018**, *8*, 422. [CrossRef]
32. Lenkovs'kyi, T.M. Fatigue Crack-Growth Resistance of Thermally Hardened 65G Steel Under Transverse Shear. *Mater. Sci.* **2017**, *53*, 200–206. [CrossRef]
33. Gao, Y.K. Fatigue Stress Concentration Sensitivity and Stress Ratio Effect of a $40CrNi_2Si_2MoVA$ Steel. *Mater. Lett.* **2017**, *186*, 235–238. [CrossRef]
34. Murakami, Y.; Yokoyama, N.N.; Nagata, J. Mechanism of Fatigue Failure in Ultralong Life Regime. *Fatigue Fract. Eng. Mat. Struct.* **2002**, *25*, 735–746. [CrossRef]
35. Sakai, T.; Sato, Y.; Oguma, N. Characteristic S–N Properties of High-Carbon–Chromium-Bearing Steel under Axial Loading in Long-Life Fatigue. *Fatigue Fract. Eng. Mater. Struct.* **2002**, *25*, 765–773. [CrossRef]
36. Shiozawa, K.; Morii, Y.; Nishino, S.; Lu, L. Subsurface Crack Initiation and Propagation Mechanism in High-Strength Steel in a Very High Cycle Fatigue Regime. *Int. J. Fatigue* **2006**, *28*, 1521–1532. [CrossRef]